

Influence of the alloying component on the protective ability of some zinc galvanic coatings

N. Boshkov^{a,*}, K. Petrov^b, D. Kovacheva^b, S. Vitkova^a, S. Nemska^b

^a *Institute of Physical Chemistry, Bulgarian Academy of Sciences, "Acad. G. Bonchev", Bl. No. 11, Sofia 1113, Bulgaria*

^b *Institute of General and Inorganic Chemistry, Bulgarian Academy of Sciences, "Acad. G. Bonchev", Bl. No. 11, Sofia 1113, Bulgaria*

Received 2 January 2005; received in revised form 2 March 2005; accepted 19 March 2005
Available online 17 May 2005

Abstract

The composition of the corrosion products of pure Zn galvanic coatings as well as of some zinc alloys (Zn–Mn and Zn–Co) after treatment in selected free aerated model media (5% NaCl and 1N Na₂SO₄) is studied and discussed. X-ray diffraction and X-ray photoelectron spectroscopy investigations are used for this purpose. It is concluded that the corrosion products (zinc hydroxide chloride hydrate in 5% NaCl and zinc hydroxide sulfates hydrates in 1N Na₂SO₄) play a very important role for the improved protective ability of the zinc alloys toward the iron substrate, compared to the pure Zn coatings. Another result is that, for a given medium, the corrosion products are one and the same for both alloys independently of the fact that the alloying component is electrically more positive or negative than the zinc. Some suggestions about the models of the appearance of these products and their protective influence are also discussed.

© 2005 Elsevier Ltd. All rights reserved.

Keywords: Corrosion; X-ray diffraction; Photoelectron spectroscopy; Zinc; Zinc alloys

1. Introduction

Zinc galvanic coating on steel substrates provides good mechanical properties, weldability, paintability as well as good corrosion resistance [1–4]. Generally, in the case of corrosion attack, zinc protects the iron or steel substrate by sacrificial protection—its layers are covered with oxidized products known as “white rust”. The corrosion resistance of zinc could be improved by using additional treatment—chromating or phosphating films, another type surface finishing or by alloying with some 3D-metals like Co, Ni, Mn, Cr and Fe [2–5]. All these alloys exhibit higher corrosion resistance (protective ability toward the substrate) compared to the individual metals [6–10].

Most of the zinc galvanic alloys used in practice contain metals that show electrically more positive potential than

the zinc itself, for example, Co, Ni, Sn, Fe and Cr. The Co is more preferred from an economical viewpoint. Considerably high protective ability in corrosion media containing Cl[−] ions or SO₂ has been reported for Co contents as low as 1–5 wt% [5,11–13]. This alloy is a solid solution of cobalt in the zinc (η -phase) with a hexagonal close packed structure.

Contrary to all above-mentioned metals, manganese has electrically more negative potential compared to the zinc and is the only metal that can be co-deposited with Zn from water solutions. High protective ability of this alloy is usually achieved at manganese amounts in the range from 40 up to 60 wt% [8,14], although lower concentrations have been also successfully used [9,10,15–17].

This article describes and specifies the protective action of the alloying component in two representative types of zinc galvanic alloys (namely, Zn–Mn and Zn–Co) during the corrosion treatment compared to the pure zinc coatings.

* Corresponding author. Tel.: +359 2 979 3920; fax: +359 2 971 26 88.
E-mail address: nbojkov@ipchp.ipc.bas.bg (N. Boshkov).

2. Experimental

2.1. Galvanic coatings (thickness $\sim 12 \mu\text{m}$, hexagonal close packed structure)

2.1.1. Zn–Mn alloy coatings

Galvanic Zn–Mn alloys were electrodeposited from a starting electrolyte (SE) (in g/l): $\text{ZnSO}_4 \cdot 7\text{H}_2\text{O}$ 10.0; $\text{MnSO}_4 \cdot \text{H}_2\text{O}$ 100.0 and $(\text{NH}_4)_2\text{SO}_4$ 60.0. The process was carried out in a double-chamber cell (500 ml volume), current density 2 A/dm^2 , pH value 5, 22°C and continuous circulation of 150 rpm. Metallurgical zinc was taken for the anodes [18]. The phase composition of these alloys is discussed and described elsewhere [18,19]. Following alloy coatings were electrodeposited and investigated:

- Zn–Mn ($\sim 6 \text{ wt}\%$), obtained by SE and two additives [18] with trade names AZ-1 (wetting agent 40 ml/l) and AZ-2 (brightener 10 ml/l). The additive AZ-1 contains poly-ethylene glycol and benzoic acid and AZ-2—benzalacetone and ethyl alcohol. This alloy forms a poly-phase coating—it consists generally in a pure zinc matrix with dispersed small zones of manganese and intermetallic compound MnZn_7 (known also as δ_1 -phase from the phase diagram of metallurgical Zn–Mn alloys) [15,18].
- Zn–Mn ($\sim 11 \text{ wt}\%$), obtained by SE and AZ-1 (20 ml/l)—the alloy contains mainly the intermetallic δ_1 -phase and small of pure zinc inclusion zones [15,18].

2.1.2. Zinc–cobalt alloy coatings

Galvanic Zn–Co (1–5 wt%) alloys are obtained by using a starting electrolyte with a composition (in g/l): $\text{ZnSO}_4 \cdot 7\text{H}_2\text{O}$ 100.0; $\text{CoSO}_4 \cdot 7\text{H}_2\text{O}$ 120.0; NH_4Cl 30.0 and H_3BO_3 25.0. The electrodepositing conditions were: current densities $2\text{--}5 \text{ A/dm}^2$, pH value 3.0–4.0, room temperature 22°C and metallurgical zinc anodes. Two laboratory additives (similar to AZ-1 and AZ-2), named ZC-1 (wetting agent 20 ml/l) and ZC-2 (brightener 2 ml/l) were also used [13].

2.1.3. Zinc coatings from a slightly acidic electrolyte

Zinc galvanic coatings were obtained from a sulfate bath containing (in g/l): $\text{ZnSO}_4 \cdot 7\text{H}_2\text{O}$ 175.0; $(\text{NH}_4)_2\text{SO}_4$ 25.0 and H_3BO_3 30.0 and deposition conditions: current density 2 A/dm^2 ; pH value 4.5–5.0; room temperature 22°C and metallurgical zinc anodes. The additives used were AZ-1 (50 ml/l) and AZ-2 (10 ml/l) [13,15].

2.2. Sample sizes and corrosion media

Both sides of steel plates with sizes $20 \text{ mm} \times 10 \text{ mm} \times 1 \text{ mm}$ were galvanically coated with pure Zn or with the alloys Zn–Mn and Zn–Co, respectively.

The protective ability of the coatings has been studied in two different corrosion media:

- model medium of free aerated 5% NaCl solution with pH ~ 6.7 at 22°C —causes mainly local corrosion;
- model medium of free aerated 1N Na_2SO_4 solution with pH ~ 6.0 at 22°C —causes local and general corrosion.

2.3. Sample characterization

2.3.1. X-ray diffraction (XRD)

The phase composition of the corrosion products was determined using X-ray diffractometer DRON-3 (Bragg–Brentano arrangement, Cu $K\alpha$ radiation and scintillation counter).

2.3.2. X-ray photoelectron spectroscopy (XPS)

The XPS measurements were carried out on an ESCALAB MkII (VG Scientific) electron spectrometer at base pressure in the analysis chamber of $1 \times 10^{-8} \text{ Pa}$ using Mg $K\alpha$ X-ray source. Pass energy of the analyzer was 20 eV and the instrumental resolution measured as the full-width at a half-maximum (FWHM) of the $\text{Ag}3d_{5/2}$ photoelectron peak is 1.2 eV. Energy scale is corrected to the C1s peak maxima at 285 eV. Sample surfaces were studied after etching with accelerated argon (Ar) ions (for depth profiling) with energy of 3 keV and ionic current of 20 mA/cm^2 .

2.3.3. Microprobe analysis

The elemental composition of the samples was determined using micro-probe analyzer JEOL Superprobe 733, Japan.

3. Results and discussion

3.1. Model medium of 5% NaCl

3.1.1. Zn–Mn alloys

3.1.1.1. X-ray diffraction. The diffraction patterns of both alloy coatings treated for 6 days in this model corrosion medium – Fig. 1B and C (Fig. 1A shows the spectra of non-treated δ_1 -phase) – contain lines of Zn, NaCl and zinc hydroxide chloride hydrate $\text{Zn}_5(\text{OH})_8\text{Cl}_2 \cdot \text{H}_2\text{O}$ (ZHC). The latter has very low product of solubility ($10^{-14.2}$) [20–22] that could be the most probable reason for the increased protective ability of this alloy, compared to the pure Zn [9,10,14,15]. It is obvious, that the coatings of the δ_1 -phase Zn–Mn ($\sim 11 \text{ wt}\%$), Fig. 1B – transform more easy to ZHC than the samples Zn–Mn ($\sim 6 \text{ wt}\%$) – Fig. 1C. Probably, the homogeneous distribution of Mn in the intermetallic coating causes the nucleation and growth of uniform ZHC layer over the whole surface.

3.1.1.2. X-ray photoelectron spectroscopy. XPS spectra of zinc and oxygen for Zn–Mn (11%) alloy before and after corrosion treatment are presented in Fig. 2. It can be seen from the Zn spectra that the peak of this metal for corrosionally non-treated sample (No. 1) occurs at binding energy $E_{\text{bind}} = 1022.5 \text{ eV}$. The literature data used [23,24], cor-

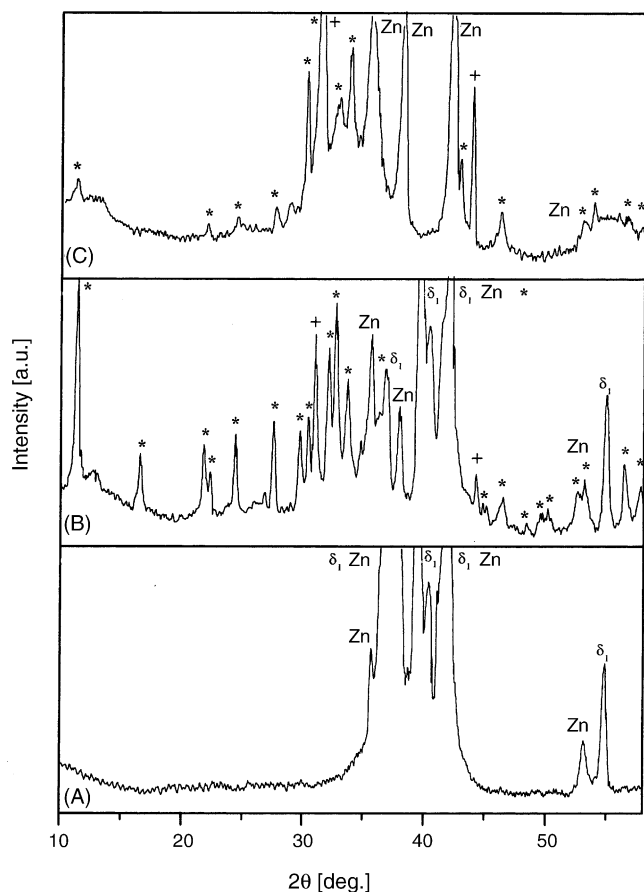


Fig. 1. Diffraction patterns in 5% NaCl solution: (A) corrosionally non-treated Zn–Mn (11 wt%); (B) Zn–Mn (11 wt%) after 6 days exposure at E_{corr} ; (C) Zn–Mn (6 wt%) after 6 days exposure at E_{corr} . (*) Diffraction lines of ZHC and (+) diffraction lines of NaCl (all plots are of the same intensity scale).

respond mainly to Zn–O bond and indicates the presence of the compound ZnO. The other sample – No. 2, corrosionally treated during 6 days at open circuit potential (OCP) – demonstrates significant changes and “splitting” of the Zn peak combined with a shift to higher E_{bind} values of 1024.4 eV. The latter could be compared to the binding energy found for Zn(OH)₂ (at 1022.6 eV) and ZnCl₂ (at 1022.5 eV) [23,24] that compounds present in ZHC (see Section 3.1.1.1).

Similar arguments could be given also for the oxygen peaks of both samples investigated. The corrosionally treated – No. 2 – coating shows a peak with greater area that suggests the appearance of newly formed compounds such as different manganese oxides as well as H₂O [23,24] (that also present in ZHC).

3.1.1.3. Double protective action of manganese. The formation of ZHC in 5% NaCl is possible only at a slight increase of the pH value of the medium [22]. Since Mn is electrically more negative element than the Zn, it dissolves first as Mn²⁺. The free electrons from the dissolution processes will react with the hydrogen ions from the medium causing a hydrogen

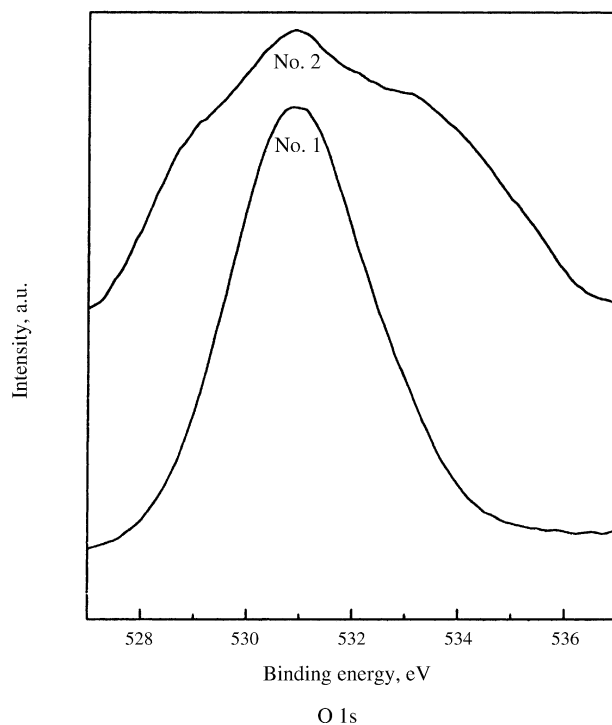
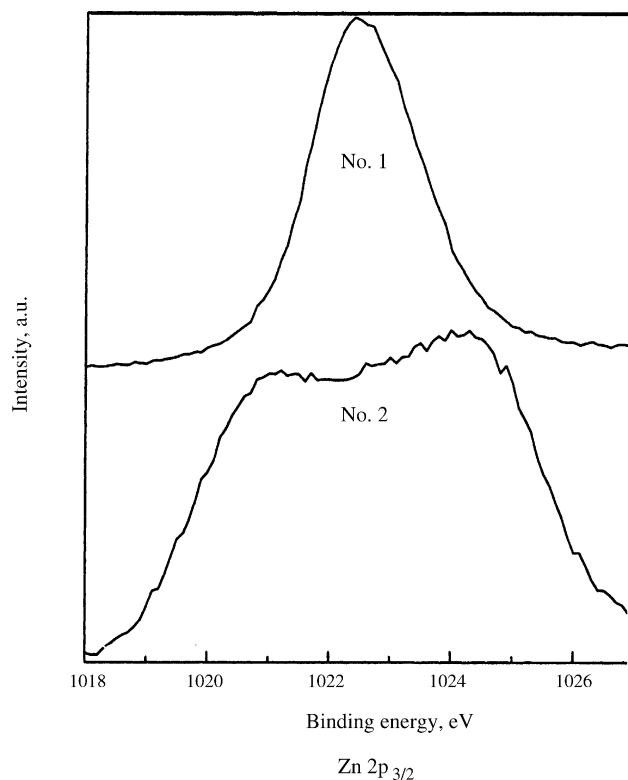


Fig. 2. Zn2p_{3/2} and O1s spectra (sputter time 10 min) of Zn–Mn (11%) alloy: No. 1, corrosionally non-treated sample and No. 2, after 6 days treatment at E_{corr} in 5% NaCl.

evolution [17,22], while some of the hydroxide OH[−] ions accumulate near the dissolved zones and breaches. As a result, the pH of the corrosion medium increases, mainly near the surface.

The spatial distribution and relative content of the different crystalline phases in the protective layer depend on the type of the deposited galvanic alloy:

- The δ_1 -phase has a very good protective ability toward the iron substrate [9,10]. Since the manganese atoms are randomly distributed in this structure they cause a forming of a compact layer of ZHC that covers almost the whole sample surface [17,19].
- In the case of galvanic alloy Zn–Mn (~6 wt%), the coating is poly-phase. The corrosion process is very intensive at the Mn/Zn interface and the manganese regions begin to dissolve. This process starts here on local surface centers and then spreads out over the whole sample. The MnZn_7 regions, which are covered with a ZHC layer, remain relatively stable—from corrosion viewpoint they, although in small quantities, act as cathode zones, scattered into the zinc phase, which is an anodic zone. Due to this distribution, considerable damages appear on the sample surface and some of the corrosion products precipitate on the cell bottom. The overall effect of the different corrosion behavior of each of the phases, consisting the coating, is the lower protective ability [17,19].
- ZHC is registered also in the presence of pure zinc during treatment in salt-spray chamber [13,17]. One of the most probable reasons for its appearance at these conditions seems to be the surface morphology. Since the galvanic coating is not perfectly smooth micro-galvanic couples appear between the protruded and concaved zones or as a result of the cathodic inclusions from the additives. The difference in this case is that the process is slower compared to both investigated Zn–Mn alloys. In addition, it can be concluded, that at these conditions of corrosion treatment and for the experimental period, ZHC does not appear in amounts that allow its XRD registration.

All these results demonstrate that the single-phase intermetallic alloy has higher protective ability against corrosion. The manganese in this coating could be formally regarded as anode protector that plays this role until it is totally dissolved. The latter process increases the pH values and causes a formation of a protective layer of ZHC. This particular mechanism, which combines anodic protection, accompanied by a formation of a layer with low product of solubility, could be regarded as a double-protective mechanism [17,19].

3.1.2. Zn–Co alloys

3.1.2.1. X-ray diffraction. The results obtained by X-ray diffraction analysis are represented on the Figs. 3 and 4 [13]. Fig. 3 shows the diffraction patterns for corrosionally non-treated samples of pure Zn (Fig. 3A) and of Zn–Co (1%) (Fig. 3B); the corrosionally treated (during 6 days exposure in 5% NaCl) Zn is shown in Fig. 3C. XRD pattern on Fig. 3A shows lines of the hexagonal zinc phase and that on Fig. 3B—of the η -phase of Zn–Co alloys (solid solution of cobalt in the matrix of hexagonal zinc), respectively. It is seen that the diffraction pattern of corrosionally treated

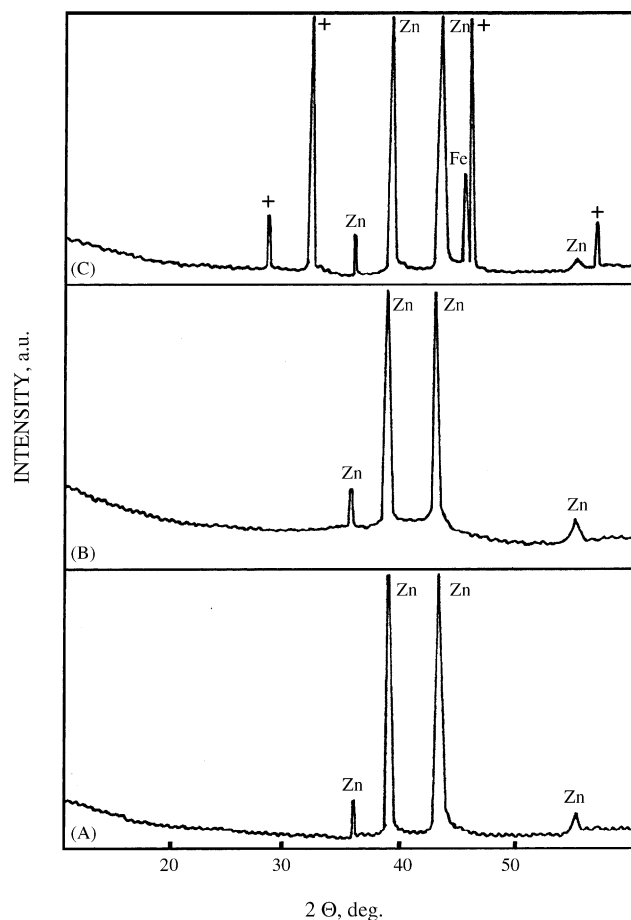


Fig. 3. Diffraction patterns in 5% NaCl solution: (A) corrosionally non-treated Zn; (B) corrosionally non-treated Zn–Co (1%); (C) galvanic Zn after 6 days exposure at E_{corr} . (+) Diffraction lines of NaCl (all plots are of the same intensity scale).

samples contains additional lines of NaCl and Fe substrate, in comparison with the non-treated ones (compare Fig. 3A and C).

XRD patterns of corrosionally treated Zn–Co (1–5%) alloy samples are shown in Fig. 4. They contain lines of the Zn–Co η -phase of the substrate, α -Fe of NaCl and also of ZHC. Its presence enhances the corrosion resistance and protective ability of the Zn–Co alloy [13] (like for Zn–Mn) compared to the pure zinc coating. The correlation “Co content/ZHC amount” can be also observed here—the intensity of the diffraction lines of ZHC gradually increases with increasing Co content (compare Fig. 4A with Fig. 4B and C). The presence of the diffraction lines of NaCl is due to the sample preparation. After the treatment, the samples were only dried in order to keep all corrosion products intact.

3.1.2.2. X-ray photoelectron spectroscopy. Fig. 5 represents the XPS spectra of zinc and oxygen for Zn–Co (3%) alloy after treatment in 5% NaCl. It can be seen that the zinc peak occurs at the binding energy $E_{\text{bind}} = 1022.9$ eV. The literature data [23,24] corroborate the presence of Zn^{2+} ions, hexa-co-ordinated by OH^- groups and of Zn^{2+} ions, tetra-co-

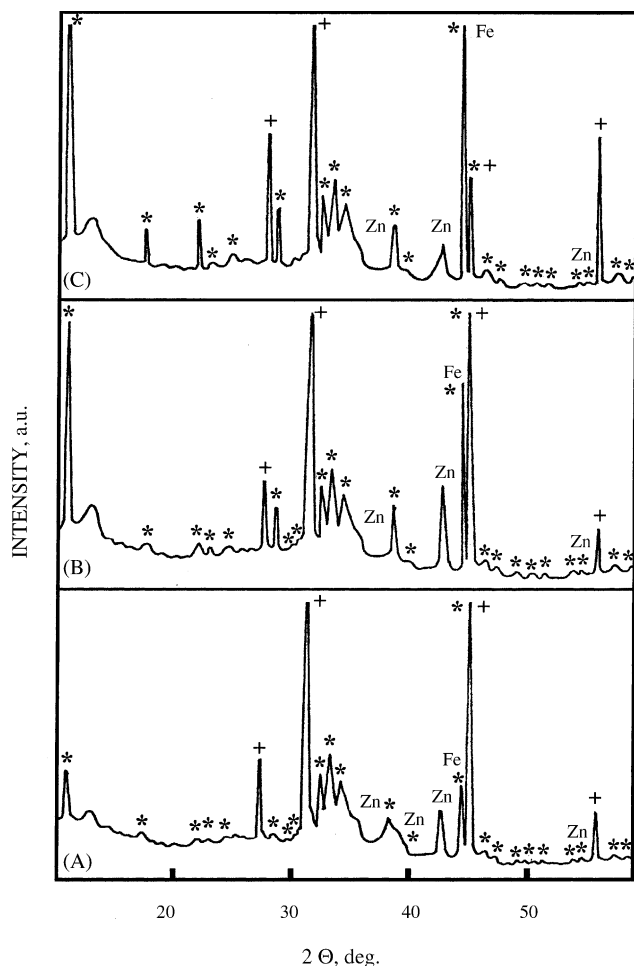


Fig. 4. Diffraction patterns in 5% NaCl after 6 days exposure at E_{corr} . (A) Zn–Co (1%); (B) Zn–Co (3%); (C) Zn–Co (5%). (*) Diffraction lines of ZHC and (+) diffraction lines of NaCl (all plots are of the same intensity scale).

ordinated by three OH^- and one Cl^- anions. These values can be compared to the binding energy found for $\text{Zn}(\text{OH})_2$ at 1022.6 eV and ZnCl_2 at 1022.5 eV. Three inner peaks appear after the computer deconvolution of the Zn spectrum. Their values are: at 1021.9 eV—corresponds to Zn–O bonds; at 1023.1 eV—corresponds to Zn–OH and Zn–Cl bonds (that present in ZHC) and at 1024.9 eV—unknown peak with low intensity. The oxygen peak registered at binding energy of 532.4 eV confirms the presence of water molecules and OH^- groups. The E_{bind} values of the inner peaks after the deconvolution are 531.0 eV (corresponds to Zn–O bonds) and 532.6 eV (corresponds to Zn–OH bonds and water molecules). All these data are conform to the elemental composition and crystal structure of ZHC.

3.1.2.3. Model of forming of ZHC and the role of Co. The results from the corrosion treatment show the presence of ZHC on the Zn–Co alloys that exhibit higher corrosion resistance and protective ability compared to the pure zinc [13]. Contrary to the Zn–Mn alloys, the process of the ZHC for-

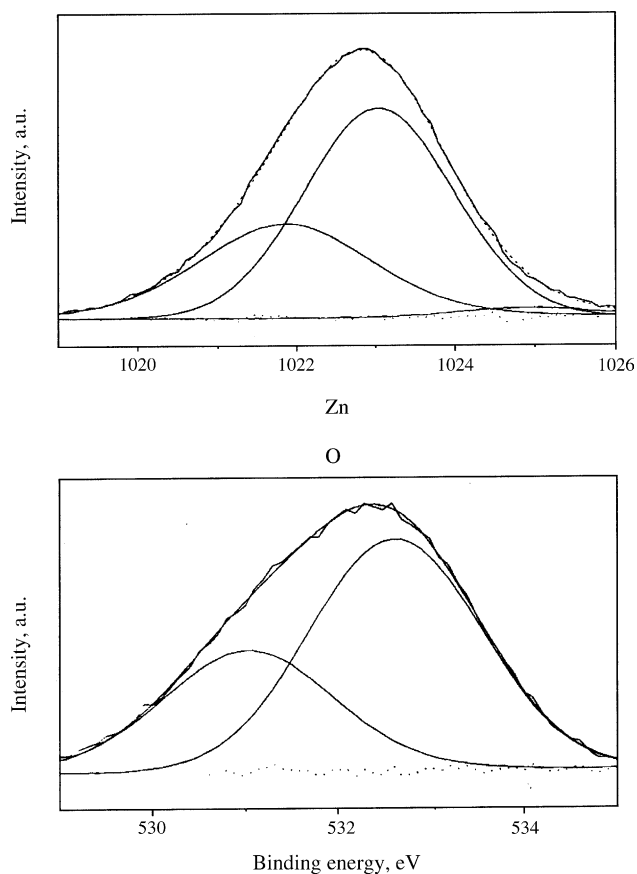


Fig. 5. XPS $\text{Zn}2p_{3/2}$ and O1s spectra (sputter time 10 min) of Zn–Co (3%) after 6 days at E_{corr} in 5% NaCl.

mation begins here with the dissolution of the Zn atoms from the alloy; those are micro-anodes when contacted with the Co atoms. The zinc begins to dissolve as Zn^{2+} ions and this process leads to appearance of free electrons, formation of neutral hydrogen atoms and hydrogen evolution. This process leads to a local increase of pH value in the depth of the corrosion damages and results in formation of zinc hydroxide chloride in the corrosion pits and their neighborhood. That is why the relative content of ZHC increases with increasing initial cobalt content.

3.2. Model medium of 1N Na_2SO_4

3.2.1. Zn–Mn alloys

3.2.1.1. X-ray diffraction. XRD patterns of samples treated during 6 days at open circuit potential E_{corr} – Fig. 6A–C – correspond to multiphase scales of hydrated zinc hydroxide sulfates (ZHS) with different degree of hydration, such as $\text{Zn}_4(\text{OH})_6\text{SO}_4 \cdot 5\text{H}_2\text{O}$, $\text{Zn}_4(\text{OH})_6\text{SO}_4 \cdot 4\text{H}_2\text{O}$, $\text{Zn}_4(\text{OH})_6\text{SO}_4 \cdot 3\text{H}_2\text{O}$, $\text{Zn}_4(\text{OH})_6\text{SO}_4 \cdot \text{H}_2\text{O}$, $\text{Zn}_4(\text{OH})_6\text{SO}_4 \cdot 0.5\text{H}_2\text{O}$, $\text{Zn}_4(\text{OH})_6\text{SO}_4$ and $\text{Zn}_7(\text{OH})_{12}\text{SO}_4 \cdot 4\text{H}_2\text{O}$ [20] as well as of Na_2SO_4 . Relative phase composition of the scales depends strongly on the condition of aging and even on ambient temperature and humidity [25]. In particular, zinc hydroxide sulfates hydrates

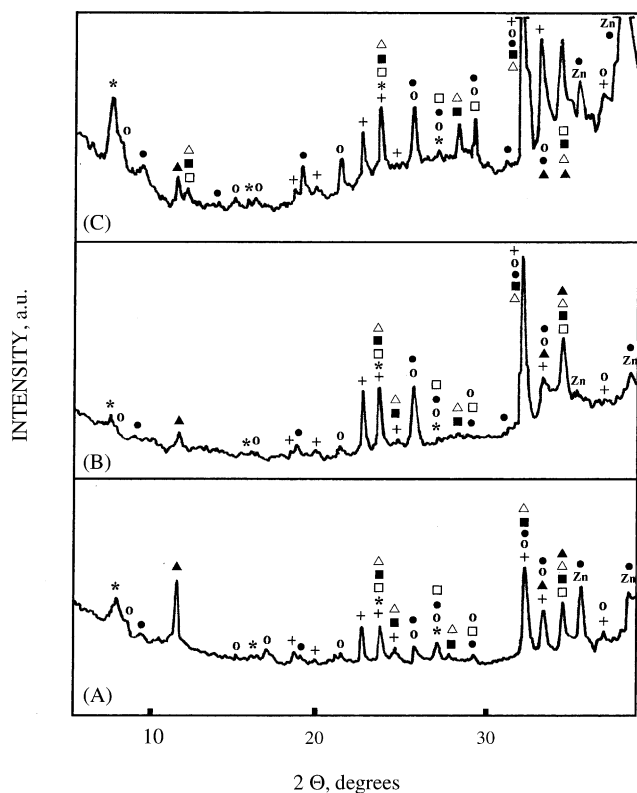


Fig. 6. Diffraction patterns of galvanic coatings after 6 days corrosion treatment at E_{corr} in 1N Na_2SO_4 : (A) pure zinc; (B) Zn–Mn (6%); (C) Zn–Mn (11%). The diffraction lines are marked off as follows: (+) Na_2SO_4 ; (□) $\text{Zn}_4(\text{OH})_6\text{SO}_4 \cdot \text{H}_2\text{O}$; (*) $\text{Zn}_4(\text{OH})_6\text{SO}_4 \cdot 5\text{H}_2\text{O}$; (■) $\text{Zn}_4(\text{OH})_6\text{SO}_4 \cdot 0.5\text{H}_2\text{O}$; (○) $\text{Zn}_4(\text{OH})_6\text{SO}_4 \cdot 4\text{H}_2\text{O}$; (Δ) $\text{Zr}_4(\text{OH})_6\text{SO}_4$; (●) $\text{Zn}_4(\text{OH})_6\text{SO}_4 \cdot 3\text{H}_2\text{O}$ and (▲) $\text{Zn}_7(\text{OH})_{12}\text{SO}_4 \cdot 4\text{H}_2\text{O}$ (all plots are of the same intensity scale).

precipitate from aqueous zinc sulfate solutions at pH values between 5.8 and 6.2. These compounds have, as a rule, very low products of solubility P_s and ensure higher protective ability of the alloy coating compared to the pure Zn [25]. For example, P_s for $\text{Zn}_4(\text{OH})_6\text{SO}_4 \cdot 4\text{H}_2\text{O}$ has a value of the order of 10^{-57} [22]. The variable amount of water molecules for a formula unit is a property inherent to their structural type.

The quantitative estimation of the relative volume fraction of the each of the ZHS phases is very difficult. The intensities of XRD lines are strongly affected by: (i) variations of water content for a formula unit, which changes even during the recording of the diagram; (ii) preferred orientation and (iii) variations of green density, etc. [25]. However, the total amount of the ZHS scales increases with increasing the Mn content in the coating. This phenomenon, observed also for Zn–Mn coatings in 5% NaCl solution, is explained with the role of Mn. Contrary to the latter case, the pure Zn coating here is also transformed in ZHS scales since their product of solubility has much lower value than that of zinc hydroxide chloride hydrate ($P_s = 10^{-14.2}$).

3.2.1.2. Model of forming of ZHS and the role of Mn. The model of formation of ZHS is probably similar to those of

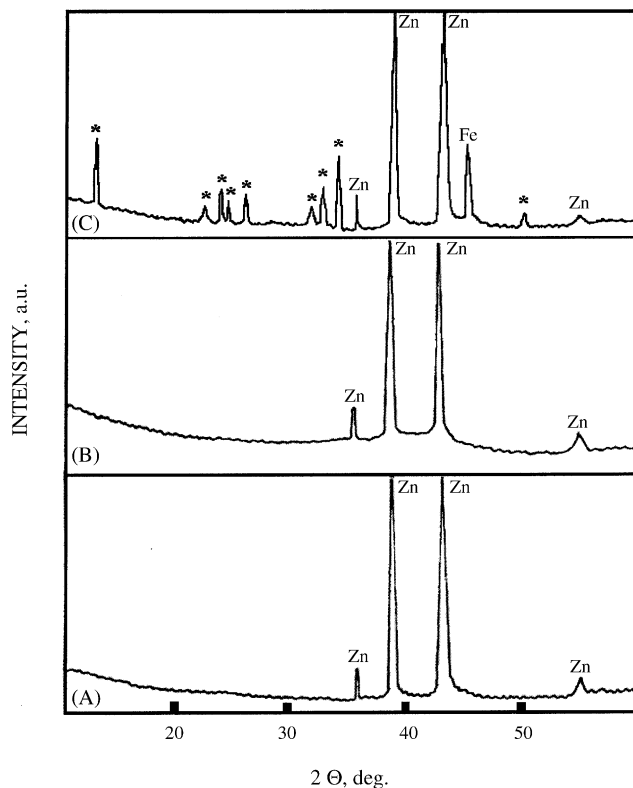


Fig. 7. Diffraction patterns in 1N Na_2SO_4 for: (A) corrosionally non-treated Zn; (B) corrosionally non-treated Zn–Co (1%); (C) galvanic Zn after 6 days exposure at E_{corr} . (*) Diffraction lines of ZHS (all plots are of the same intensity scale).

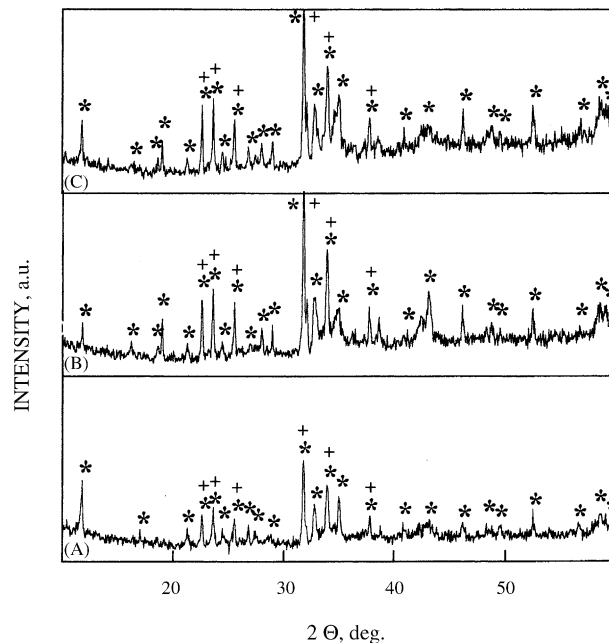


Fig. 8. Diffraction patterns in 1N Na_2SO_4 after 6 days exposure at E_{corr} : (A) Zn–Co (1%); (B) Zn–Co (3%); (C) Zn–Co (5%). (*) Diffraction lines of ZHS and (+) diffraction lines of Na_2SO_4 (all plots are of the same intensity scale).

ZHC—dissolution of the electrically more negative manganese, increasing of pH value and appearance of ZHS. The extent of protection might be not the same due to the fact that the types of ZHS compounds could easily transform in their different variants (depending on the conditions) that is unfavorable from corrosion viewpoint. Contrary to the similar experiments in 5% NaCl, corrosion products with low P_s are registered here also on pure Zn during the investigated period although in small amounts.

3.2.2. Zn–Co alloys and Zn

3.2.2.1. X-ray diffraction. The results obtained by XRD analysis are represented on the Figs. 7 and 8. Fig. 7 demonstrates the diffraction patterns for corrosion non-treated samples of pure Zn (Fig. 7A) and of Zn–Co (1%) (Fig. 7B) as well as corrosion treated (during 6 days exposure in the medium) Zn (Fig. 7C). On Fig. 7A – lines of the hexagonal zinc phase can be seen and on Fig. 7B – the η -phase of Zn–Co alloys. The differences in the diffraction patterns of the corrosion non-treated and treated galvanic samples of pure Zn consist here not only in the lines of Fe and of the corrosion medium (like in 5% NaCl) on the treated one, but also in the presence of ZHS, marked with an asterisk (com-

pare Fig. 7A and C). XRD patterns of corrosion treated Zn–Co (1–5%) alloy samples are shown in Fig. 8. They contain lines of Na_2SO_4 and also of different compounds of ZHS (marked with an asterisk). The formation and the role of ZHS have been already discussed in the case of Zn–Mn. The correlation “Co content/ZHS amount” is demonstrated with the intensity of the diffraction lines of ZHS that gradually increases with increasing Co content (compare Fig. 8A, on one hand, with Fig. 8B and C, on the other hand).

3.2.2.2. X-ray photoelectron spectroscopy. Fig. 9 represents the XPS spectra of zinc and oxygen for Zn–Co (3%) alloy after corrosion treatment. Fig. 9 shows a Zn “splitting” for the zinc peak that occurs at $E_{\text{bind}} = 1022.0$ and 1023.5 eV. From the literature data [23,24] used, it could be concluded that these values correspond to the presence of ZnO as well as sulfates in higher amounts. Three inner peaks appear after the computer deconvolution of the Zn spectrum. Their values correspond to Zn metal (1021.5 eV) and Zn–O bonds

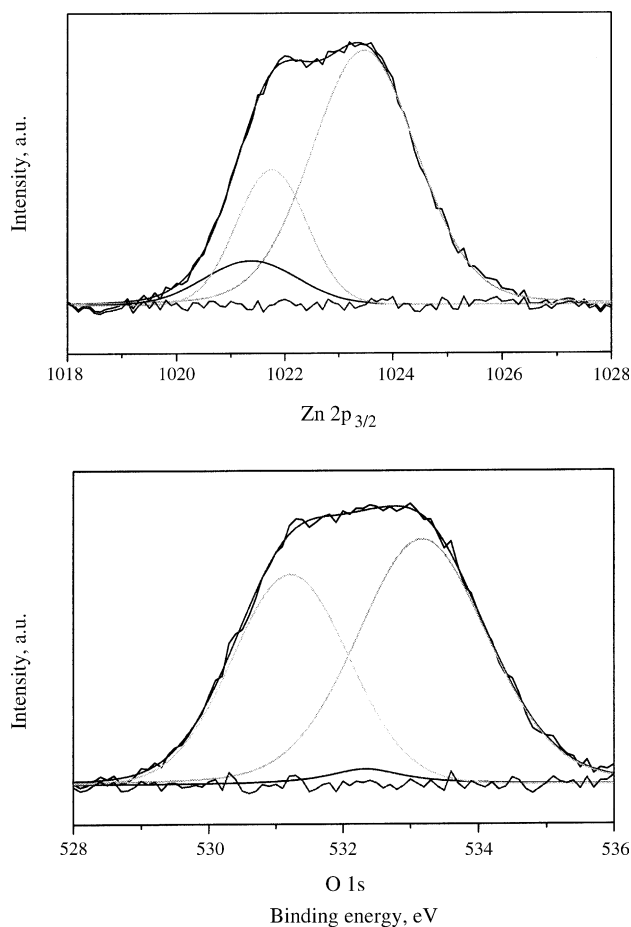


Fig. 9. XPS $\text{Zn}2p_{3/2}$ and $\text{O}1s$ deconvoluted spectra (sputter time 10 min) of Zn–Co (3%) alloy after 6 days at E_{corr} in 1N Na_2SO_4 .

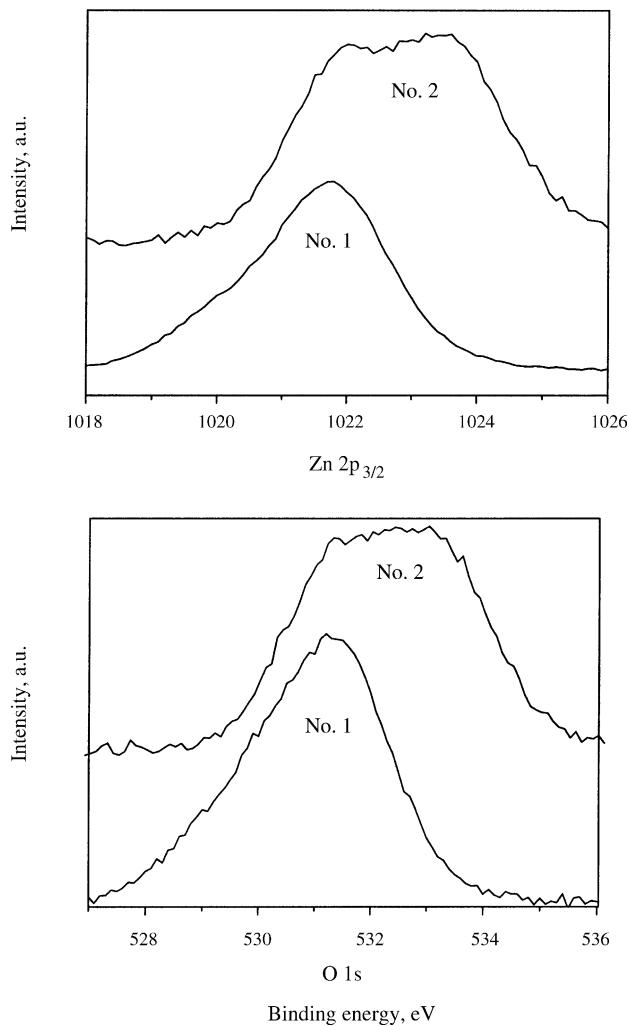


Fig. 10. XPS $\text{Zn}2p_{3/2}$ and $\text{O}1s$ spectra (sputter time 10 min) of Zn and Zn–Co (3%) alloy after 6 days at E_{corr} in 1N Na_2SO_4 . No. 1, Zn and No. 2, Zn–Co (3%).

(1021.8) and this at 1023.5 eV to sulfates (that present in ZHS). The oxygen peak registered at binding energies between 531.3 and 533.0 eV confirms the presence of oxides, water molecules and hydroxide (OH^-) groups. The E_{bind} values of the inner peaks after the deconvolution are 531.2 eV (corresponds to Zn–O bonds) and 533.2 eV (corresponds to Zn–OH bonds and water molecules). All these data are conform to the elemental composition and crystal structure of ZHS.

Fig. 10 demonstrates the comparison of Zn $2p_{3/2}$ and O1s XPS spectra (sputter time 10 min) of corrosionally treated during 6 days in this model medium at E_{corr} samples of Zn and Zn–Co (3%). It could be concluded that for one and the same time of exposition at equal conditions the Zn spectrum of the alloy (sample No. 2) is larger and wider (shifted to higher E_{bind} values) that is a sign for higher ZHS amounts in this case. Similar is the situation with the O spectrum (sample No. 1, pure Zn sample) is brief (condensed) compared to the spectrum of the alloy. The latter demonstrate a shift to higher E_{bind} that correspond to greater amounts of oxides, hydroxides and H_2O .

3.2.2.3. Model of forming of ZHS and role of Co. The model is analogical to the formation of ZHC in the Zn–Co alloys in 5% NaCl. Contrary to the Zn–Mn alloys this process begins with the dissolution of the Zn atoms from Zn–Co alloys that are micro-anodes compared to the Co atoms. This process leads to a local increase of pH value in the depth of the corrosion damages and has as a result the formation of ZHS in these places.

4. Conclusions

Following conclusions, based on the results obtained, can be done:

- (1) The increased protective ability of some Zn alloys (Zn–Mn and Zn–Co) toward iron substrate compared to the pure zinc coatings is a result of the appearance of corrosion products with low product of solubility after the treatment—ZHS (in 1N Na_2SO_4) and ZHC (in 5% NaCl). This effect seems to be more pronounced in 1N Na_2SO_4 due to the presence of different types ZHS. The results in 5% NaCl confirm the appearance only of ZHC. The models of forming of these compounds are different for both alloy types although the final result is the same.
- (2) The structure of the alloy is of great importance. For example, the uniformly distribution of the alloying component in the Zn matrix ensures the formation of compact ZHC or ZHS layers on the substrate.
- (3) Manganese has a double-protective action—on one hand, it dissolves first as the more negative element protecting the Zn and on the other, ensures the forming of ZHC, respectively, on the galvanic coating.
- (4) The formation of hydroxo-salts on Zn during corrosion treatment is well known phenomenon. Generally, this process can be stimulated (for example, in the galvanic alloys) by the presence of an element (metal) that is electrically more negative than the zinc. Thus, the corrosion products form and grow as a result of the sacrifice corrosion of the alloying component itself. The same products, however, can appear provided the alloying component is electrically more positive than the zinc—in this case, they form as a result of corrosion (dissolution) of Zn itself. Contrary to the first case, this event may be regarded as “self-sacrifice” protection.

References

- [1] A.M. Ginsberg, A.F. Ivanova, L.L. Kravchenko (Eds.), *Galvanotekhnika, Manual, Metallurgija, Moscow, 1987.*
- [2] M. Sagiyama, T. Urakawa, T. Adanija, T. Hara, Y. Fukuda, *Plat. Surf. Fin.* 11 (1987) 77.
- [3] S. Mueller, M. Sarret, T. Andreu, *J. Electrochem. Soc.* 149 (11) (2002) 600.
- [4] M.R. Lambert, R.G. Hart, *SAE Tech. Pap.* 860 (1986) 266.
- [5] W.M.J.C. Verberne, *Trans. IMF* 64 (1986) 30.
- [6] D. Lay, W. Eckles, *Plat. Surf. Fin.* 9 (1990) 10.
- [7] M. Kurpjoweit, *Galvanotechnik* 85 (1994) 3252.
- [8] G. Loar, K. Romer, T. Aoe, *Plat. Surf. Fin.* 78 (1991) 74.
- [9] N. Boschkov, G. Raitschevski, S. Vitkova, *Metalloberflaeche* 53 (7) (1999) 27.
- [10] N. Boschkov, G. Raitschevski, Tz. Tzatscheva, S. Nikolova, *Metalloberflaeche* 53 (8) (1999) 32.
- [11] J.S. Zhang, Z.L. Yang, M.Z. An, W.L. Li, Z.M. Tu, *Plat. Surf. Fin.* 5 (1995) 135.
- [12] G.D. Wilcox, D.R. Gabe, *Corros. Sci.* 35 (1993) 1251.
- [13] N. Boshkov, K. Petrov, S. Vitkova, S. Nemska, G. Raichevski, *Surf. Coat. Technol.* 157 (2–3) (2002) 171.
- [14] G. Govindarajan, V. Ramakrishnan, S. Ramamurthi, V. Subramanian, N.V. Parthasaradhy, *Bull. Electrochem.* 5 (1989) 422.
- [15] N. Boshkov, S. Vitkova, K. Petrov, *Met. Fin.* 99 (9) (2001) 56.
- [16] N. Boshkov, St. Nemska, S. Vitkova, *Met. Fin.* 100 (5) (2002) 14.
- [17] N. Boshkov, K. Petrov, S. Vitkova, *Met. Fin.* 100 (6) (2002) 98.
- [18] N. Boschkov, K. Petrov, S. Nikolova, S. Vitkova, *Metalloberflaeche* 52 (7) (1998) 514.
- [19] N. Boshkov, *Surf. Coat. Technol.* 172 (2003) 217.
- [20] Joint Committee on Powder Diffraction Standards—Powder Diffraction Files No. 7-155.
- [21] W. Nowacki, J.H. Silverman, *Z. Kristallographie* 21 (1961) 115.
- [22] J. Rasines, Thesis Doctoral, Universidad de Madrid, Facultad de Ciencias, Serie A, No. III, Seccionde Quimicas, Madrid, 1970.
- [23] G.E. Muilenberg (Ed.), *Handbook of X-ray Photoelectron Spectroscopy*, Eden Prairie, Minesota, Perkin-Elmer Corp., Physical Electronics Division, 1994.
- [24] V.I. Nefedov, *Rentgeno-electroskopija Chimicheskich Soedinenii, Chimija, Moskwa, 1984.*
- [25] N. Boshkov, K. Petrov, S. Vitkova, G. Raichevski, *Surf. Coat. Technol.* 194 (2–3) (2005) 276.